The 2009 IEEE/RSJ International Conference on
Intelligent Robots and Systems
October 11-15, 2009 St. Louis, USA

Antagonistic and Series Elastic Actuators: a Comparative Analysis on the Energy Consumption

M. Laffranchi[1,2], N.G.Tsagarakis[1], F. Cannella[1], and D.G.Caldwell[1]

[1]Italian Institute of Technology (IIT), Genova 16163, Italy

[2]The University of Sheffield, Western Bank Sheffield, S10 2TN, UK

Abstract—**Recent investigations show that compliant systems can be more safe and energy-efficient than conventional stiff actuated systems. As a result, researchers are increasingly implementing compliance within actuation systems using a variety of mechanisms. In general, these actuators can be grouped in 2 main categories. The first category includes all the actuation systems with a compliant element connected in series (SEA), while the second group contains all those systems that employ two actuators placed antagonistically. In both designs the ability to regulate the stiffness is essential in order to meet safety and/or performance demands. Energy consumption is a very important aspect to be considered, especially in autonomous robots. This paper presents a theoretical study on the energy consumption of variable stiffness actuators, comparing the amount of energy required in order to perform a certain task.**

I. Introduction

MUSCLES and tendons change their stiffness as a function of the motion/task they have to perform. Arm muscles assume a stiff configuration when the arm has to perform an accurate task, while they are compliant when they are performing the "loading" phase of a throw. Similarly, if we analyze jumping we see that leg muscles are compliant during the "loading" phase of the jump or during the landing phase where they absorb the shock [1], while during the "pushing" phase, they are stiff. There are several reasons for this variation in stiffness but among the most pressing is the exploitation of the elastic energy stored within the muscles and tendons [2]. This enables compliant actuators to achieve performance which is not possible with a conventional stiff robotic system. In [3] it has been shown that there is a clear difference between the velocities of the links and the throw distances obtained in the two cases. Clearly the introduction of compliance may have very significant effects on the performance of an actuation system relative to the classical stiff design.

As a result robotics researchers are starting to investigate these effects and include compliance within robots. Sometimes energy saving is considered as a non-priority issue, even though, if autonomous robots are of concern, this feature is one of the most important. In this paper a study on the energy consumption of elastic joint actuators is presented.

This paper is structured as follows: Section II reports on the two main configurations of a compliant actuated joint and Section III presents the models of these two configurations. The simulation methods are presented in Section IV, while in Section V the value of the stiffness of the human elbow during a throwing task is determined. Section VI reports on the design of the nonlinear spring used in the models of the elastic actuated joints with simulation results presented in Section VII. Finally Section VIII addresses the conclusion.

II. Classification of Compliant Joint Actuators

Compliant actuation systems can be categorized into two main groups: so-called Series Elastic Actuators (SEA) [4], [5], [6], and the antagonistically-actuated joints [7], [8], [9].

A. Antagonistic Design

Antagonistically-actuated joints employ two compliant elements to provide power to the joint. This design is biologically-inspired, since mammalian anatomy follows the same concept, i.e. a joint actuated by two muscles arranged in an antagonistic manner. The muscle-tendon cooperation gives the driven link (arm, leg etc) a controllable and variable compliance. In addition to biological muscle this type of antagonistic compliance controlled can be achieved

Matteo Laffranchi is with the Italian institute of Technology (IIT), Genova 16163, Italy (e-mail: Matteo.Laffranchi@ iit.it) and within the University of Sheffield, S10 2TN, UK.
N.G.Tsagarakis is with the Italian institute of Technology (IIT), Genova 16163, Italy (phone: +39 010 71781 428; e-mail: nikos.tsagarakis@ iit.it).
F. Cannella[1]is with the Italian institute of Technology (IIT), Genova 16163, Italy (e-mail: Ferdinando.Cannella@ iit.it)
D.G.Caldwell is with the Italian institute of Technology (IIT), Genova 16163, Italy (e-mail: darwin.caldwell@ iit.it).

using both conventional two motor electric drive designs and other more biologically inspired forms such pneumatic Muscle Actuators (pMA). In the latter case compliance is an inherent characteristic of the actuator, while for an electrical design compliant elements (generally springs) have to be embodied into the system [7-10].

B. Serial Design (SEA)

The series elastic actuator is characterized by the mechanical series, motor–gear–compliant element and has been implemented both in linear and rotational designs [4], [5], [6]. This paper will study a rotational SEA.

III. THE MODELS OF THE ELASTIC JOINT ACTUATORS

This section presents the dynamic models of the two elastic joint configurations discussed in the previous section.

A. Antagonistic configuration

An antagonistically-actuated joint uses two driving elements. The stiffness of the joint and the angular displacement of the driven link are set by means of a combination of the actuation inputs q1, q2 (see Fig. 1). By co-contraction of these actuators, preloading and, thus, tuning of the stiffness is achieved, while the rotation of the joint is obtained by the antagonistic motion of the drives.

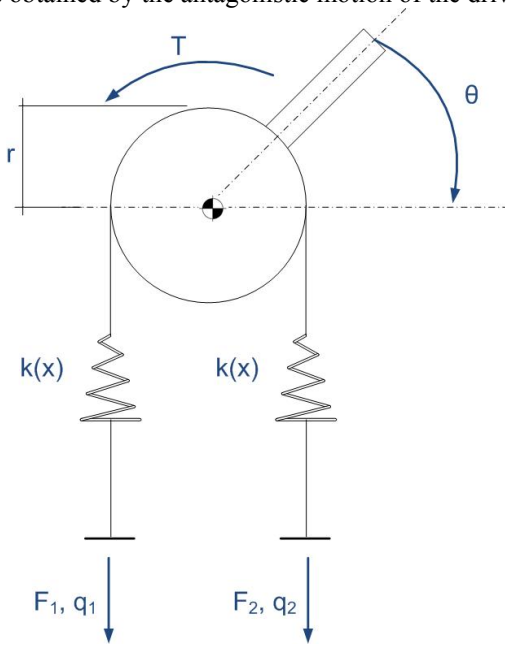

Fig.1 Antagonistic setup.

The static equilibrium equation for the torque at the joint, excluding gravitational forces, is:

$$T = r \cdot (F_1 - F_2) \tag{1}$$

For the first drive:

$$F_1 = (\theta \cdot r + q_1) \cdot k_1(q_1, \theta) \tag{2}$$

The equilibrium equation at the second actuator is:

$$F_2 = (-\theta \cdot r + q_2) \cdot k_2(q_2, \theta) \tag{3}$$

Now, assuming a quadratic relationship between the compression and the force generated by the spring

$$k_1(q_1, \theta) = k_{rate}(q_1 + \theta \cdot r) + k_{offset} \tag{4}$$

$$k_2(q_2, \theta) = k_{rate}(q_2 - \theta \cdot r) + k_{offset} \tag{5}$$

Differentiating (1) with respect to the angle θ, the torsion stiffness of the joint is obtained:

$$k_{tors} = \frac{dT}{d\theta} = (k_{rate} \cdot q_1 + k_{rate} \cdot q_2 + k_{offset}) \cdot 2 \cdot r^2 \tag{6}$$

Assuming J as the moment of inertia of the output link, the dynamic equation for the output link is:

$$J \cdot \ddot{\theta} + (F_1 - F_2) \cdot r = 0 \tag{7}$$

From (6), q_1 as a function of q_2 and k_{tors} is obtained:

$$q_1 = \frac{k_{tors} - (k_{offset} + k_{rate} \cdot q_2) \cdot 2 \cdot r^2}{2 \cdot k_{rate} \cdot r^2} \tag{8}$$

Finally, by substituting (8), (2), (3) in (7), the motion to be generated by the actuator input q_2, as a function of $\theta, \ddot{\theta}$ *and* k_{tors}, is obtained.

$$q_2 = \frac{\left(4 \cdot \theta \cdot r^3 \cdot k_{rate} \cdot k_{tors} + k_{tors}^{\ 2} + 4 \cdot \ddot{\theta} \cdot J \cdot r^3 \cdot k_{rate} - 2 \cdot k_{tors} \cdot r^2 \cdot k_{offset}\right)}{4 \cdot k_{rate} \cdot k_{tors} \cdot r^2} \tag{9}$$

From (8) and (9), it is possible to obtain q_1, q_2 as a function of θ and k_{tors} (Fig. 2).

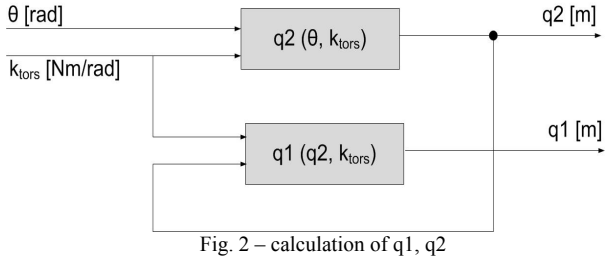

Fig. 2 – calculation of q1, q2

B. Serial configuration

The design of a SEA can be represented by the series combination "motor–gearbox–elastic element–link" where the stiffness varies as a function of the preload on the compliant elements. Figure 3 shows conceptually a SEA with adjustable variable stiffness. The effort needed to drive the link is given by T_{in}, while θ_{in} is the angle of the input pulley. The torque generated by the motor that adjusts the stiffness of the joint is T_{ktune}, and θ_{ktune} is the preload of the

compliant element. The output angle is θ_{out}. As with the antagonistic setup, this design presents three control variables: the driving shaft angular displacement θ_{in}, the driven shaft angular displacement θ_{out} and the angular displacement of the stiffness tuning system θ_{ktune} which adjusts the preload of the spring.

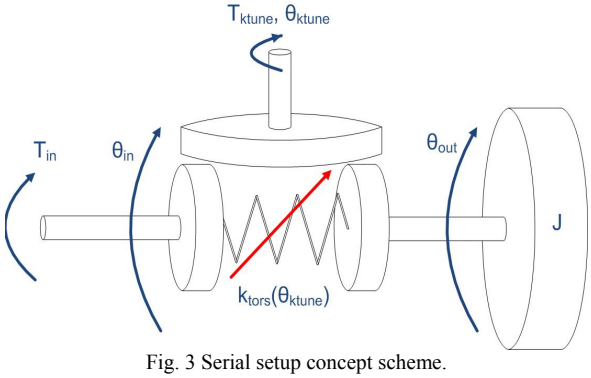

Fig. 3 Serial setup concept scheme.

To provide a fair comparison with the antagonistic configuration, a series rotational compliant element which is inspired by the antagonistic setup is simulated where the springs like the output pulley characteristic do not change, Fig. 4.

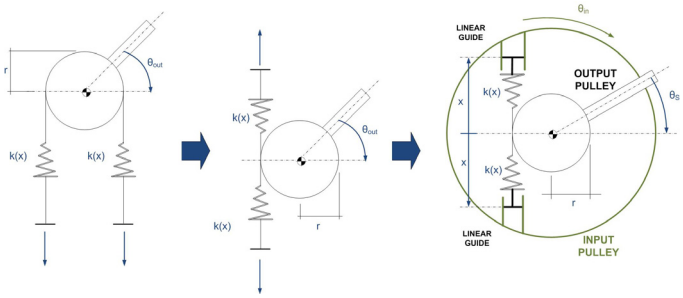

Fig. 4 From the antagonistic to the serial configuration.

From the kinematics of the system $\theta_{in} + \theta_S = \theta_{out}$, where θ_S is the deflection of the compliant element. Writing the Newton-Euler equation for the serial system as in Fig. 3, the equilibrium equation for the driving pulley, excluding gravitational forces, is obtained:

$$T = (\theta_{in} - \theta_{out}) \cdot k_{tors}(\theta_{in}, \theta_{out}) \tag{10}$$

To ensure fairness when compared with the antagonistic setup, and to make the energy consumption independent of the system design, a mass-less driving pulley is considered. The driving pulley, thus, has to work only against the torque generated by the spring. For the outer link:

$$J \cdot \ddot{\theta}_{out} + (\theta_{out} - \theta_{in}) \cdot k_{tors}(\theta_{out}, \theta_{in}) = 0 \tag{11}$$

Substituting (10) in (11), the equation of the torque required by the system to achieve a given output motion is:

$$T = J \cdot \ddot{\theta}_{out} \tag{12}$$

To tune the stiffness, a certain preload has to be applied to the springs. The resultant preload force is

$$F_{tune} = 2 \cdot k(x) \cdot x_{tune} \tag{13}$$

Where *k(x)* is the stiffness of the springs. The torque developed due to the input-output angle difference is:

$$T = (-\theta_{in} + \theta_{out}) \cdot 2 \cdot k(x) \cdot r^2 \tag{14}$$

For an infinitesimal input-output angle difference, (14) becomes $dT = 2 \cdot k(x) \cdot r^2 \cdot d\theta$ and the torsional stiffness of the system is then:

$$k_{tors}(x) = \frac{dT}{d\theta} = 2 \cdot k(x) \cdot r^2 \tag{15}$$

From this equation the desired linear stiffness of the spring can be calculated as a function of the torsion stiffness:

$$k(x) = \frac{k_{tors}(x)}{2 \cdot r^2} \tag{16}$$

The equation that models the behavior of the stiffness during spring compression (see also section VI) is

$$k(x) = k_{rate} \cdot x + k_{offset} \tag{17}$$

This assumption is almost correct if the spring is preloaded to work in its quadratic region. The displacement to be imposed on the system to achieve a required stiffness can then be obtained as follows.

$$x = \frac{k(x) - k_{offset}}{k_{rate}} \tag{18}$$

Substituting (16) in (18) the spring preload is obtained.

$$x = \frac{\frac{k_{tors}(x)}{2 \cdot r^2} - k_{offset}}{k_{rate}} \tag{19}$$

The force developed to reach the preload calculated in (19) is given by (13). From these equations the work done due to the stiffness tuning is computed, while from (12) the torque to calculate the work done for the dynamic task is obtained.

IV. SIMULATIONS

This section describes how the simulators for the two designs are implemented. In order to make a comparative study that is independent of the physical characteristics of the actuator and the design, the torque and the velocity generated are unlimited, with infinite bandwidth, and the driving pulleys are mass-less. The transmission bodies are rigid while friction and damping are not considered in this study. These assumptions are obviously far from reality, but are made to make the model independent of the design of the system. We can summarize the characteristics of the models as follows:

i) Linear (no saturations, no dead zones, no friction).
ii) No damping.
iii) Massless actuators.
iv) Rigid and massless transmission bodies.

The models used for the simulations take into account the variation of the moment of inertia due to the releasing of the ball during the throw. The following moments of inertia are computed assuming that the bodies are pointmasses. The moment of inertia calculated at the elbow, due to the complex forearm is computed as:

$$J_{forearm} = m_{forearm} \cdot l_{COG\_forearm}^{\ 2} = 1.254 \cdot (0.11)^2 kg \cdot m^2 .$$

The position of the center of mass, the weight and the dimensions of the forearm are reported in [11], [12].

The moment of inertia at the elbow, due to the hand is $J_{hand} = m_{hand} \cdot \left(l_{forearm} + l_{COG\_hand}\right)^2 = 0.47 \cdot (0.257 + 0.095)^2 kg \cdot m^2$

While the moment of inertia computed at the elbow, due to the ball, assuming that the center of mass of the ball is aligned with the center of mass of the hand, is $J_{ball} = m_{ball} \cdot \left(l_{forearm} + l_{COG\_hand}\right)^2 = 0.15 \cdot (0.257 + 0.095)^2 kg \cdot m^2$

When the ball is held by the thrower, the total moment of inertia is $J_{total\_before} = J_{forearm} + J_{hand} + J_{ball}$ while when the ball is thrown the inertia becomes $J_{total\_after} = J_{forearm} + J_{hand}$

The value of the moment of inertia with respect to the joint is set equal to the value of J_{total_before} during the first phase, when the ball is grasped with the hand, while after the release it is set to J_{total_after}. The models from section III are implemented in simulation to compute the physical variables of the systems during the task execution and the results are used to compare the two design configurations.

A. Antagonistic Setup

The model of the antagonistic setup receives the trajectory of both the angle and the stiffness of the joint as input and outputs the work done by the system. In Fig. 5, the block called "Inverse Kinematics - ODE" obtains q_1, q_2 as a function of a desired output trajectory and stiffness as in (8), (9). The "Inverse Dynamics" block implements (2), (3). The work due to each actuation input is computed, and the total work is obtained as the sum of each work.

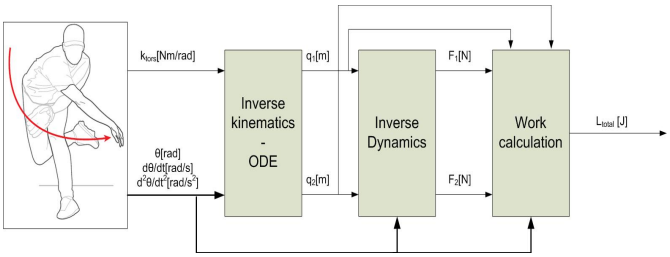

Fig. 5 Concept block diagram for the antagonistic setup simulator.

The work performed by the driving link "1" is:

$$W_{q1} = \int P_{q1} \cdot dt = \int F_1 \cdot \dot{q}_1 \cdot dt \tag{20}$$

Similarly, the work for the driving link "2" is:

$$W_{q2} = \int P_{q2} \cdot dt = \int F_2 \cdot \dot{q}_2 \cdot dt \tag{21}$$

The total work is the sum of (20) and (21)

$$W_{total} = W_{q1} + W_{q2} \tag{22}$$

B. Serial Setup

Figure 6 shows the block diagram of the serial setup simulator, using the trajectory of both the angle and the stiffness of the joint as inputs, and returning the work done.

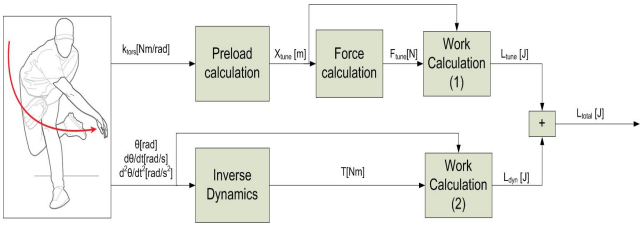

Fig. 6 Concept block diagram for the serial setup simulator.

The block called "Preload calculation" computes the spring preload to deliver certain stiffnesses, according to (19). The block called "Force calculation" implements equation (13). The block called "Work calculation (1)" computes the energy consumption by integrating the power.

$$W_{tune} = \int P_{tune} \cdot dt = \int F_{tune} \cdot \dot{x}_{tune} \cdot dt \tag{23}$$

The block "Inverse Dynamics" implements the inverse dynamics of the joint as in (12). Hence, the work to perform the motion is

$$W_{dyn} = \int P_{dyn} \cdot dt = \int T \cdot \dot{\theta} \cdot dt \tag{24}$$

The total work is the sum of (23) and (24).

$$W_{total} = W_{tune} + W_{dyn} \tag{25}$$

V. STIFFNESS AND ANGLE TRAJECTORY

The trajectory of the elbow of the dominant arm of male subjects during fast baseball throws can be found in [13]. This trajectory, which is shown in Fig. 7, is one of the inputs given to the simulator.

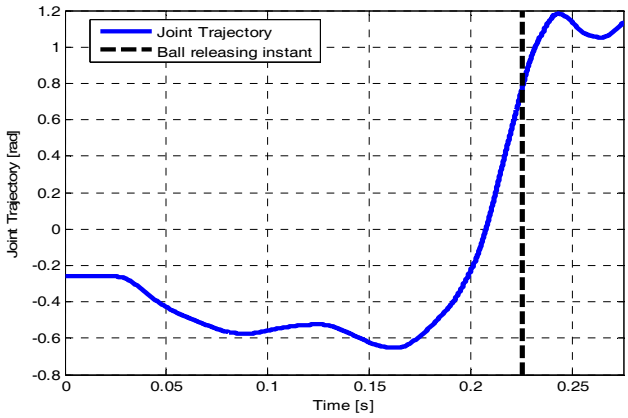

Fig. 7 Elbow rotation during a fast baseball throw.

It can be seen that in the loading phase (0÷0.16s) the elbow performs a backward motion. The ball is pushed forward until the instant in which the ball is released (0.225s). In the last phase the elbow rotation velocity decreases in order to stop the forearm after the throw. In this paper, the motion of the elbow in the space during the execution of the task is not considered. The calculation of the stiffness of the joint is therefore related to a baseball pitch performed with the elbow kept fixed to rotate around a fixed axis.

A. Stiffness trajectory

The stiffness of the joint is the second input given to the simulator. For the case of a fast baseball pitch, the elbow rotation data have been used to compute the torque applied to the joint during the execution of the task by computing the inverse dynamics as in (12). Plotting the torque versus the angle of the elbow joint, the stiffness of the joint during the different phases of the pitch is obtained, Fig. 8. This method for the stiffness calculation has been used in [14].Three different phases can be observed in Fig. 8:

i. Pushing phase with increasing torque (positive power)
ii. Pushing phase with decreasing torque (positive power)
iii. Braking phase (negative power)

For each phase, a value of the stiffness of the joint has been obtained. These three values, for the fast throw case are shown in Table I. The first phase can be interpreted as a compression spring that is being loaded (positive increasing effort and positive flow), the second phase can be considered as a compression spring that is releasing its energy (positive decreasing effort and positive flow), while the third phase can be seen as a tension spring that is pulling (negative decreasing effort, positive flow). The profile of the stiffness as a function of the time is then imposed as a piecewise-constant function that assumes constant values during each section described.

TABLE I
STIFFNESS VALUES FOR THE FAST THROW CASE

Phase	Stiffness[Nm/rad]
Phase 1	124
Phase 2	252
Phase 3	549

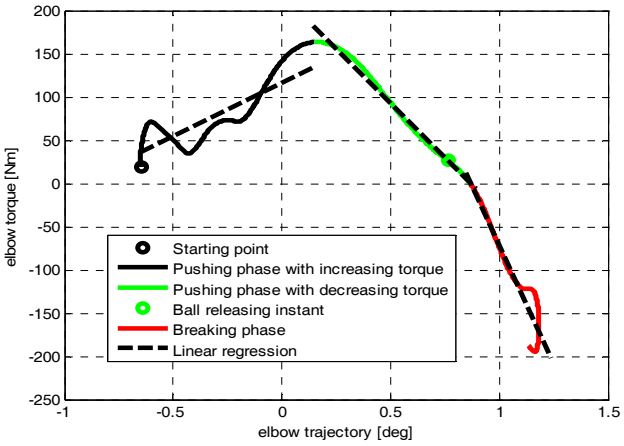

Fig. 8 Torque vs angle for a fast throw.

VI. SPRING DESIGN

The spring to be used in the models has to be nonlinear in order to allow the tuning of the stiffness of the joint. In order to achieve this characteristic, conical helical springs were designed to provide stiffness variability within the range computed for the human elbow. Considering a radius of $r = 50mm$ for the driven pulley for both models, the range of stiffness that the spring has to provide in order to emulate the human elbow stiffness in the task execution is obtained using (16).

$$k_{lin\_\min} = \frac{k_{tors\_\min}}{2 \cdot r^2} = \frac{124}{2 \cdot (50 \cdot 10^{-3})^2} = 24.8 \frac{kN}{m}$$

$$k_{lin\_\max} = \frac{k_{tors\_\max}}{2 \cdot r^2} = \frac{549}{2 \cdot (50 \cdot 10^{-3})^2} = 109.8 \frac{kN}{m}$$

A spring that can achieve these values of stiffness has been designed. FEM simulations have been performed to characterize the spring force-compression relationship. The spring parameters are reported in Table II while the force-compression curve is shown in Fig. 9

The stiffness of the spring as a function of the compression can be obtained by differentiating the force with respect to the compression, Fig. 10. It can be noticed

that the last part of the range of compression of the spring makes the stiffness almost linear with the compression. This means that the force is approximately quadratic with the compression. This assumption has also been made in [15].

The linear regression applied to this section returns the following values, referring to (17):

$$k_{rate} = 2.4 \cdot 10^{7}\, N \cdot m^{-2}; koffset = -4.3 \cdot 10^{5}\, N \cdot m^{-1}$$

TABLE II
SPRING PROPERTIES

Elastic Modulus of the material [MPa]	206000
Poisson Coefficient	0.33
Wire diameter [mm]	3
D_0 [mm]	13.5
D_u [mm]	29.5
L [mm]	42
Maximum Compression [mm]	22.5

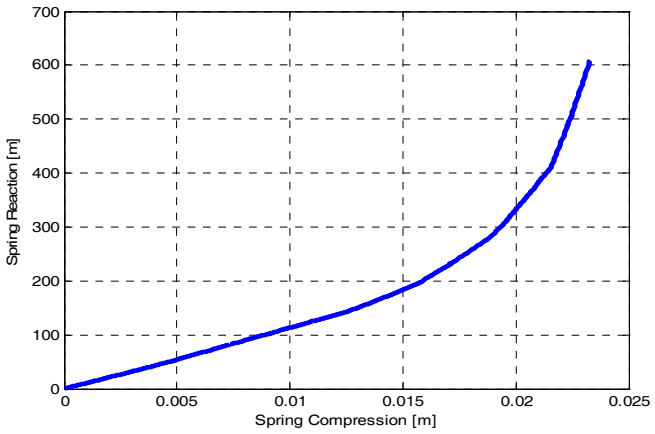

Fig. 9 Force-Compression relationship of the conical spring.

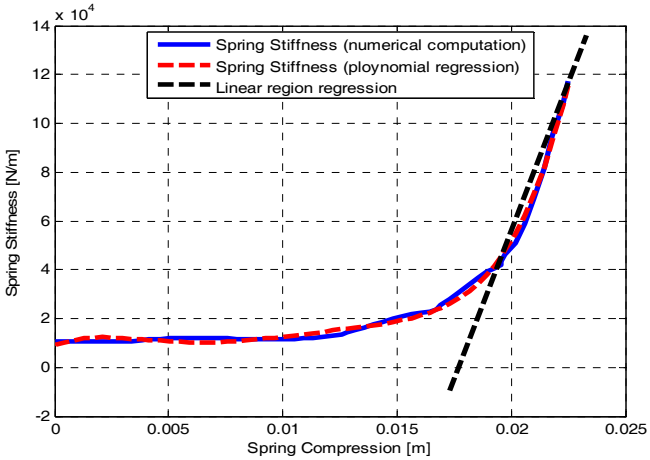

Fig. 10 Spring Stiffness as a function of the compression.

VII. Simulation Results

The results obtained from the simulation study of the two models show that there are differences between the models in terms of energy consumption. This difference can be observed in Fig. 11, after the ball releasing instant. The input work is calculated as the sum of the work required to execute the motion and the work required to adjust the stiffness.

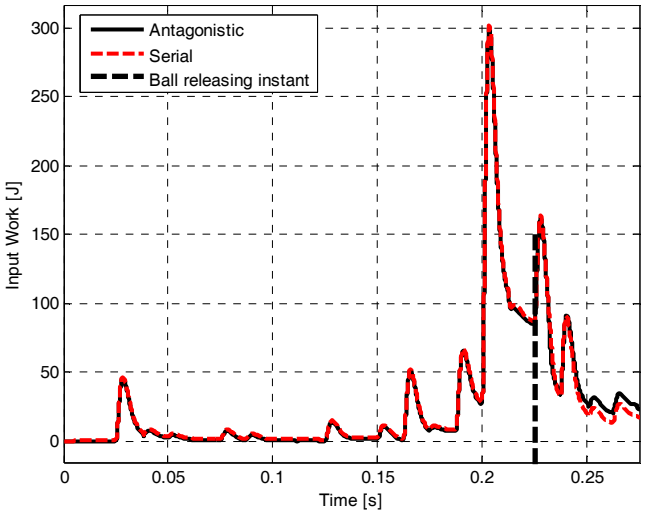

Fig. 11 Work required from the different designs to compute the task.

The energy consumption levels for the antagonistic and the serial setup are reported in Table III.

TABLE III
ENERGY CONSUMPTION

Setup	Energy consumption [J]
Antagonistic setup	26.5
Serial setup	19

In the case of the antagonistic setup the energy consumption is about 40% more than that of the serial setup. This implies that the serial setup is a more efficient configuration than the antagonistic setup.

In Fig. 12 it is possible to notice that the power provided to the system is positive until approximately 0.01s before the releasing of the ball. After releasing the ball the power given to the system decreases suddenly to its minimum. This occurs because the releasing of the ball is followed by a braking phase.

In Fig. 13 the energy stored in the two actuator designs is shown. The energy stored is obtained as the difference of the energy provided to the system and the work done by the link: $W_{stored} = W_{in} - W_{out}$. What is interesting to notice is that in both cases the energy stored reaches the maximum at time t=0.203s and after that it is transferred to the output just before the release of the ball. A difference of energy (required, Fig. 11 and stored, Fig. 13) is noticeable only after the ball releasing instant. It is possible to see that the energy provided to the serial system is exploited entirely to perform the motion of the outer link (the energy stored into the system is zero at the final time), while, at the end of the task, an amount of energy is stored into the antagonistic setup. This difference is equal to the difference of the

required energy from the two systems at the final instant. This is equal to $\Delta W \approx 7.5J$. This means that the extra energy required for the antagonistic setup is retained in the system and more specifically in the springs of the antagonistic setup.

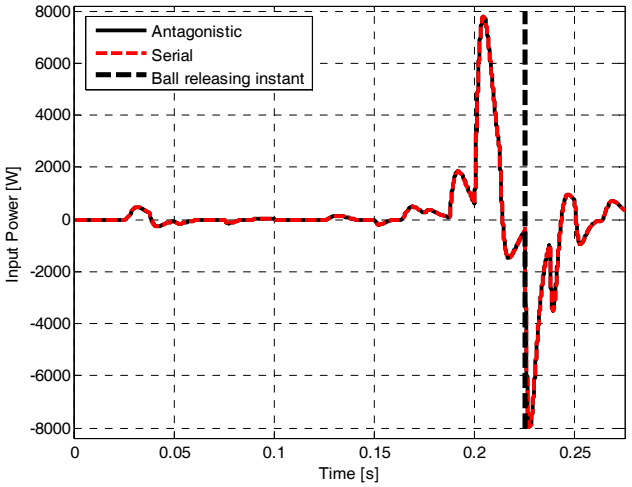

Fig. 12 Power provided for the different designs.

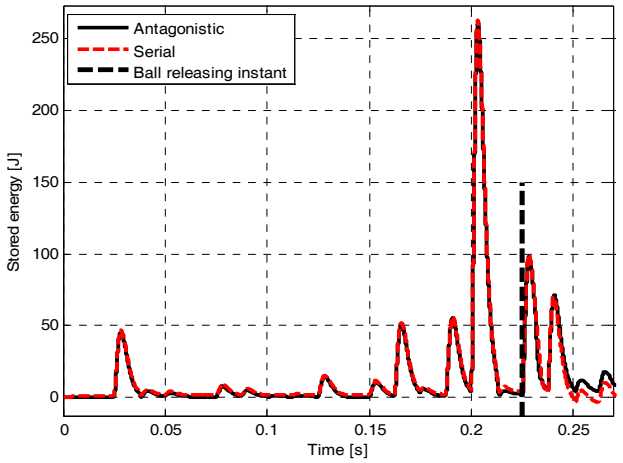

Fig 13 Energy stored into the different actuator designs.

VIII. CONCLUSIONS AND FUTURE WORK

In this paper a study of the energy consumption of two designs of elastic actuators was presented. In particular, an antagonistically-actuated joint and a series elastic actuator joint were evaluated. Models of the two configurations were presented. The value of the stiffness of the elbow during the execution of a task (i.e. the elbow performs a fast throw of a baseball) was obtained to tune the stiffness of the two joints emulating the biological behavior of the elbow during the throwing of the ball.

Simulation results were presented, comparing the differences of the two configurations in terms of the energy required and the energy storage. These results reveal that the antagonistic setup requires more energy with respect to the serial in order to execute the same task.

Future work include the evaluation of the influence of the parameters of the systems, e.g. moment of inertia of the actuator, friction, viscous damping, in terms of energy efficiency. Further studies encompass the analysis of the energy consumption of the articulation of the upper limbs for other tasks. The same investigation will be done for the lower limb articulations for gait/jumping task.

ACKNOWLEDGMENT

This work is supported by the VIACTORS European Commission FP7-ICT-2007-3 project.

REFERENCES

[1] J. Tak-Man Cheung, M. Zhang, K.N. An, "Effects of plantar fascia stiffness on the biomechanical responses of the ankle-foot complex", Clinical Biomechanics 19, 2004

[2] M. Ishikawa, P.V. Komi, M.J. Grey, V. Lepola, G.P. Bruggemann, "Muscle-tendon interaction and elastic energy usage in human walking", Journal of applied physiology 99, 2005.

[3] S. Wolf and G. Hirzinger, "A new variable stiffness design: matching requirements of the next robot generation", IEEE International Conference on Robotics and Automation, Pasadena, CA, USA, 2008

[4] Pratt G. and Williamson M., "Series elastic actuators", Proceedings of IEEE/RSJ International Conference on Intelligent Robots and Systems, 1995, vol. 1, pp. 399–406.

[5] N.G. Tsagarakis, M. Laffranchi, B. Vanderborght and D.G. Caldwell, "A Compact Soft Actuator Unit for Small Scale Human Friendly Robots", 2009 IEEE International Conference on Robotics and Automation Kobe, Japan, May 2009

[6] M. Zinn, O. Khatib, and B. Roth, "A new actuation approach for human friendly robot design", The international journal of robotics research, Vol. 23, No.4-5, April-May 2004, pp. 379-398

[7] B. Vanderborght, B. Verrelst, R. Van Ham, M. Van Damme, P. Beyl and Dirk Lefeber, "Development of a compliance controller to reduce energy consumption for bipedal robots", Autonomous Robots, Springer, February 2008.

[8] D.G. Caldwell, N. Tsagarakis, D. Badihi and G.A. Medrano-Cerda, "Pneumatic Muscle Actuator Technology: a light weight power system for a Humanoid Robot", IEEE International Conference on Robotics and Automation, Leuven, Belgium, May 1998.

[9] S.A. Migliore, E.A. Brown, S. P. DeWeerth, "Biologically Inspired Joint Stiffness Control", IEEE International Conference on Robotics and Automation, Barcelona, Spain, April 2005

[10] A. Bicchi, S. Lodi Rizzini, G Tonietti, "Compliant Design for intrinsic safety: General issues and preliminary design", IEEE International conference on robots and systems, Maui, Hawaii, USA, 2001

[11] A.R. Tilley, H.D. Associates, "The Measure of Man and Woman: Human Factors in Design", Whitney Library of Design, 1993

[12] D. Winter, "Biomechanics and motor control of human movement", New York Wiley, 1990

[13] J. Hore, M. O'Brien, S. Watts, "Control of Joint Rotations in Overarm Throws of Different Speeds Made by Dominant and Nondominant Arms", Journal of Neurophysiology 94, 2005

[14] C.J. Walsh, "Biomimetic design of an under-actuated leg exoskeleton for load-carrying augmentation", MS thesis, Massachussets Institute of Technology, 2006

[15] A. Bicchi, G. Tonietti, "Fast and "Soft-Arm" Tactics", IEEE Robotics and Automation Magazine, 11 (2), 12-21.